Light Scattering Study of Structures in a Smectic Liquid Crystal

Abstract: The effect of surface treatment, sample thickness, and cooling rate on the structural order in the smectic phase of p-noctyl-p'-cyano-biphenyl has been investigated by light scattering, and the results have been interpreted in terms of theories developed for crystalline polymers. Fan-shaped superstructures are found when the long dimension of the liquid crystal molecules is aligned parallel to the wall of a cell. But banded two-dimensional spherulites exist when the long dimension of the molecules is aligned perpendicular at one wall and parallel at the opposite wall. Uniaxially oriented rodlike structures are observed when the wall surface is lapped. Because surfaces have a strong effect, the superstructures are less highly ordered in thick than in thin cells. With an increase in cell thickness, the size of the superstructures increases along with the degree of disorder. If a sample is cooled rapidly to the solid state and then heated to the smectic state, the order in the smectic liquid crystal is reduced, as shown by a marked increase in the effect of density fluctuations on light scattering patterns. In a sample cooled slowly from the nematic to the smectic state, light scattering results primarily from orientation fluctuations.

Introduction

Liquid crystals, as the name implies, are characterized by the existence of molecular order intermediate between that of the liquid and crystalline states. The nature of such order has been used to classify liquid crystals into three categories-smectic, nematic, and cholesteric-each of which reflects a different type of local molecular organization [1, 2]. The order in these phases, at short range, derives from parallel or nearly parallel arrangements of elongated and fairly rigid molecules. This short-range order, characteristic of the distance between molecules and layers of molecules, as well as the orientation of molecules with respect to each other, can be measured by xray scattering. The correlation distance, which is a measure of the range of the order, is observed to be less than a few tens of nanometers. The actual short-range order, however, can extend to distances on the order of 100 nm or more. The x-ray studies become difficult because the xray scattering associated with such long correlation distances occurs at very small angles, which for experimental purposes are difficult to access. These large-ordered domains do, however, scatter visible light at much larger angles and thus present no experimental difficulties to characterization by the light scattering techniques. The xray scattering is primarily sensitive to the electron density of the systems and is only indirectly related to the molecular orientation. On the other hand, the light scattering is dependent on the anisotropy of the system, which is determined by the type and orientation of the chemical bonds constituting the molecules. The description of the arrangement of these bonds is of prime importance in describing structures in liquid crystals.

The light scattering technique has been widely used for structural characterization in crystalline polymers [3]. The interpretation of structural information has been based on two approaches, the model approach and the statistical approach. The model approach is suited to systems that have definite structural units; it provides information about the shape and size of these structures. The statistical approach is applied to systems that cannot be characterized by a discrete model; the structural information is thus described by statistical parameters. Both of these approaches have been applied to structural characterization of liquid crystals [4–9]. For example, Stein et al. [4] showed that the solid state of certain cholesteryl esters can exist either in a negatively birefringent spherulitic form with a size dependent on crystallization temperature

Copyright 1978 by International Business Machines Corporation. Copying is permitted without payment of royalty provided that (1) each reproduction is done without alteration and (2) the *Journal* reference and IBM copyright notice are included on the first page. The title and abstract may be used without further permission in computer-based and other information-service systems. Permission to republish other excerpts should be obtained from the Editor.

(model approach), or in the form of randomly correlated aggregates of crystals best characterized by a correlation function (statistical approach).

In this work, we have used light scattering to investigate the structures in the smectic phase of p-n-octyl-p'-cyanobiphenyl and the variations in these structures due to surface effects, sample thickness, and thermal history.

Experimental

• Material and cell preparation

The liquid crystal, p-n-octyl-p'-cyanobiphenyl, was obtained from Gallard-Schlesinger Chemical Corporation, New York. The transition temperature, for the state change from solid to smectic, $T_{\rm ss}$, is 19.48°C (292.63 K); from smectic to nematic, $T_{\rm sn}$, it is 32.60°C (305.75 K); and from nematic to isotropic, $T_{\rm NI}$, it is 39.54°C (312.69 K), as measured by differential scanning calorimetry.

Cells for light scattering studies were formed by placing a spacer of 13 µm between two sheets of 0.50-cm-thick glass that was filled with the liquid crystal and then sealed with an epoxy-covered Mylar TM (E. I. du Pont de Nemours & Co.). The glass was treated to obtain different alignments of the liquid crystal at its surfaces. A parallel alignment with the cell surface was obtained by either coating the glass with plasma-deposited SiO_a or by lapping the glass with AB gamma alumina #3 for two minutes on a wheel 18 in. (45.72 cm) in diameter. The homeotropic alignment was achieved by plasma-depositing a polyfluorocarbon film onto the substrate [10]. A cell with mixed alignment, i.e., parallel alignment at one cell surface and perpendicular alignment at the opposite surface, was constructed with one SiO₃-coated glass and one polyfluorocarbon-coated glass. This mixed-alignment cell is similar to that reported by Kahn [11].

In order to study the structure dependence on cell thicknesses, a wedge-shaped cell was constructed by placing a spacer between two sheets of glass along one edge and placing the two sheets in contact with each other along the opposite edge. The surface treatment was the same as that of the mixed-alignment cell.

The designations and descriptions of these cells are summarized in Table 1.

Cells, after being filled with the liquid crystal, were heated to 38° C (311.15 K) to convert the system into the nematic state. Reversion of the liquid crystal to the smectic phase was then accomplished by allowing the cell to cool by natural convection to ambient temperature (about 23° C or 296 K). In this manner, the possibility of non-uniform filling of cells was avoided. The thermal treatments to the samples involved different degrees of superheating and rates of cooling carried out in a Mettler FP-52 hot stage. For the superheating treatment, a sample was heated to 10, 20, and 30 K above the T_{Ni} and then

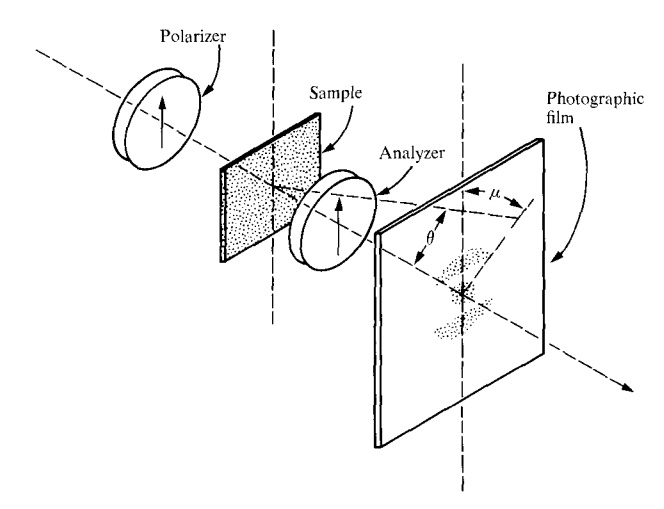


Figure 1 Schematic diagram of a photographic light scattering apparatus (from [16]).

Table 1 Description of sample cells.

Sample cell	Surface treatment	Alignment	Thickness (μm)
A	polyfluorocarbon coated	perpendicular	13.0
В	SiO ₂ coated	parallel	13.0
C	lapped	parallel	13.0
D	combined*	mixed	13.0
E	combined*	mixed	variable

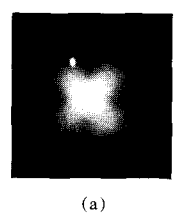
^{*}One surface coated with SiO2; the other surface coated with polyfluorocarbon

cooled slowly to 296 K. Two cooling rates were applied to the samples. The slow-cooled sample was made by cooling the sample from the nematic state to the smectic state by natural convection and the fast-cooled sample was obtained by quenching the sample from the nematic state with liquid nitrogen and then allowing it to slowly reach 296 K.

• Light scattering experiment

A photographic light scattering apparatus was used to record scattering patterns. A schematic diagram of the apparatus is shown in Fig. 1. The light source was a Spectra Physics Model 133-01 helium-neon laser equipped with a Spectra Physics Polarization rotator whose power and wavelength are 1.0 mW and 632.8 nm, respectively. The scattering patterns were recorded on Polaroid Type 52 films, ASA400.

In a light scattering experiment, two types of polarization arrangement are generally used. The H_{ν} pattern is obtained when the polarizer and analyzer are perpendicular to each other and the V_{ν} pattern is obtained



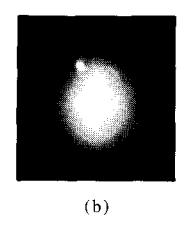




Figure 2 Scattering patterns and photomicrograph of SiO_2 coated cell. (a) H_{ν} ; (b) V_{ν} ; and (c) photomicrograph between crossed polaroids, with the enclosed center portion a schematic representation of optic axis orientation.

when the polarizer and analyzer are parallel. The H_v scattering arises mainly from orientation fluctuations, while the V_v scattering derives from both orientation and density fluctuations [12]. In this work, mainly H_v patterns were employed to interpret the structures found in the liquid crystal samples. Polarizing photomicroscopy was used to complement structural information obtained from light scattering patterns.

Results and discussion

• Effect of surface treatment

Sample cell A (see Table 1), with the liquid crystal homeotropically aligned, appeared to be clear and the scattered light intensity was too weak to be recorded. The cell, when observed between crossed polaroids on a polarizing microscope, was not totally dark but appeared to be light greyish-blue in color. Such a "homeotropic blue" has been observed in cholesteryl myristate and was attributed to the scattering of visible light by structures of sizes smaller than the wavelength of the light [9]. The homeotropic alignment in sample cell A must have caused the elongated molecules to orient parallel to the optical paths (cell surface normal to the incident light beam) and thus reduced the scattering cross section of the aggregates formed, resulting in a very weak scattering state.

The H_v and V_v scattering patterns from sample cell B are shown in Figs. 2(a)–(d). The H_v pattern appears to be a superposition of two similar scattering patterns, a very bright one at low angles and a weaker one extended to larger angles. While the low-angle H_v pattern may be expected from randomly oriented rods [13], such structures do not seem to closely represent the fanlike structure observed in the photomicrograph [Fig. 2(c)]. Yoon [14] and Tatematsu et al. [15] have shown that such patterns can also be obtained from structures having a single sheath-like or sector shape. When the sector angle is greater than 120°, the patterns are characteristic of spherulite scattering; e.g., there exists an intensity maximum in the H_v clover-leaf lobe [16]. When the sector angle is less than 120°,

as in the fan-shaped structure in Fig. 2(c), the scattering patterns are like those from rod scattering. Thus, the lowangle patterns observed from sample cell B can best be interpreted as coming from large fanlike structure instead of from rods. A closer look at Fig. 2(c) shows that within a fanlike region, there are short striations of different shades, which indicate a variation in orientation of the optic axis. The fluctuation in orientation has a strong correlation along the striation and thus may be describable by the "nonrandom orientation fluctuations" theory [17, 18]. In such a system, the probability that the optic axes a, and a, (Fig. 3) of two scattering elements are parallel depends on the separation vector \mathbf{r}_{ij} and the angle $\boldsymbol{\beta}$ between one of the axes and \mathbf{r}_{ii} . When β is close to 0° , the optic axes tend to be parallel to the long direction of the correlated domain and form the so-called fiberlike structure. When β is close to 90°, a disklike structure is formed. Such a system is different from one described by "random orientation fluctuations" [19] in that the correlated orientation in the "random" systems depends only on the separation of the optic axes and thus usually gives rise to spherical domains. Schematic representations of the random, fiberlike, and disklike orientation correlations are shown in Figs. 4(a)-(c). The scattering patterns obtained from systems with random orientation fluctuations are cylindrically symmetric about the incident beam. The scattering from both fiberlike and disklike structures results in the same four-fork H, pattern. However, in the case of disklike structures, the V, pattern is extended longer in the direction parallel to the polarizer; while for fiberlike structures, extension is in the direction perpendicular to the polarizer. In Fig. 2(b) the wide angle V. pattern extends farther in the direction perpendicular to the polarizer, suggesting that the structure in the striation is fiberlike. The orientation of the optic axis was further verified by determining the slow axis of the correlated regions within a sector by using a polarizing microscope. The slow axis was found to lie along the striation. Since the polarizability anisotropy of the liquid crystal is positive [20], the liquid crystal domain thus can be assumed to lie parallel to the long direction of the striation, a condition which results in fiberlike correlated domains. Such fiberlike correlated domains are smaller than the host fanlike structure and are responsible for the wideangle scattering pattern [Fig. 2(a)], since these smaller scattering domains will scatter at larger angles. The schematic representation of the orientation of the optic axis within the fanlike structure is shown in the enclosed center portion of Fig. 2(c). The dark edge between the fanlike structures and the different shades of the striation within the fanlike structure result from the change in orientation of the optic axis.

The H_v pattern from sample cell C, with the lapping direction close to the polarizer direction, is shown in Fig.

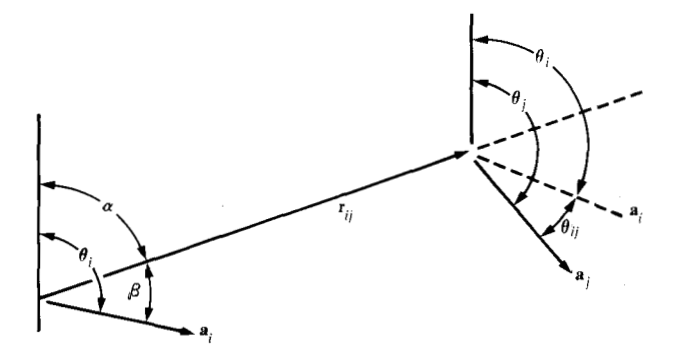


Figure 3 The angles α , β , and θ_{ij} for two scattering elements with their optic axes oriented at angles θ_i and θ_j and separated by \mathbf{r}_{ij} in two dimensions (from [18]).

5(a). The pattern shows a long streak extending in a direction perpendicular to the lapping direction. The pattern rotates with the rotation of sample; that is, the streak remains extended perpendicular to the lapping direction, as shown in Figs. 5(b) and 5(c), in which the lapping direction is parallel to and at 45° to the polarizer direction, respectively. The scattered light intensity in Fig. 5(c) is much stronger than that observed in Figs. 5(a) and 5(b). A 5× shorter exposure time must be used to record Fig. 5(c), so that the streak will not be washed out through overexposure. Diffuse scattering at wide-angle could be observed in the Fig. 5(c) arrangement if the normal exposure time were used. Such diffuse scattering could not be observed from the arrangements shown in Figs. 5(a) and 5(b) even if a much longer exposure time were used.

Figure 5(d) shows long fiberlike structure extended mainly in the lapping direction, indicating a highly anisotropic orientation for the structure. The H_v pattern shown in Fig. 5(a) can be reproduced by the theoretically calculated pattern [Fig. 6(a)] obtained by using the Stein-Rhodes rod theory [13]. The theory is based on scattering from independent rods without consideration of the scattering interference from other rods. However, for qualitative structural identifications, the theory has been successfully applied to systems having either randomly distributed or oriented rods [13, 21]. The calculated pattern consists of five intensity levels spaced uniformly in the logarithmic scale between the maximum and the minimum shown by the markers in the order of $0 > \Delta > + >$ $X > \spadesuit$. In the calculation a delta function is used to describe the orientation distribution of rods; i.e., the probability of finding a rod oriented in one particular direction, the lapping direction, is the greatest, while that for any other direction is almost zero. The pattern in Fig. 5(b) can also be calculated [Fig. 6(b)] by taking the maximum orientation direction to be at 90° to the polarizer direction. Thus, the structure in sample cell C can be described as consisting of uniaxially oriented rods, in agreement with the structure shown in Fig. 5(d).

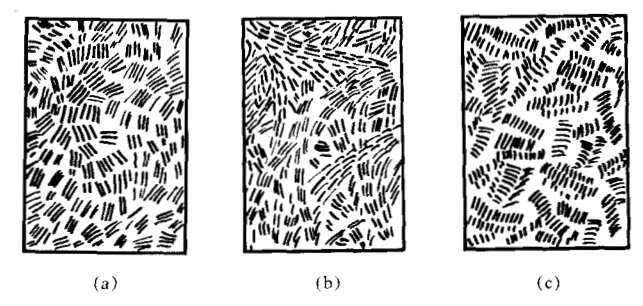


Figure 4 Schematic of (a) random, (b) fiberlike, and (c) disklike correlation in orientation (from [19]).

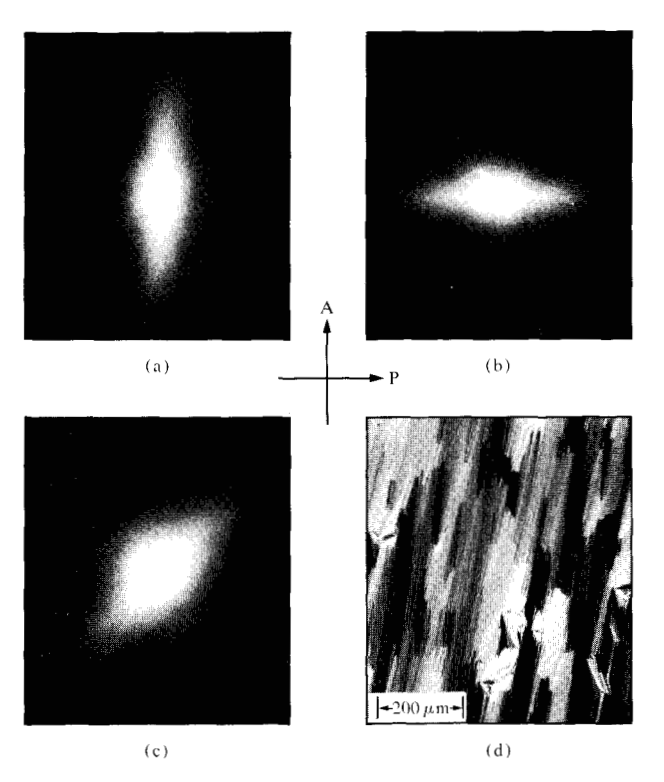


Figure 5 H_v scattering patterns and photomicrograph of lapped cell. (a) Lapping direction parallel to analyzer; (b) lapping direction parallel to polarizer; (c) lapping direction at 45° to polarizer; (d) photomicrograph between crossed polaroids.

When the optic axis of these rods is at 45° to the polarizer or analyzer, two effects can be expected. First, the scattered light intensity is increased. This is because the induced dipole is a vector quantity, and the magnitude of the observed scattered intensity depends on the component of the vector with respect to the polarization direction of the analyzer. When the optic axis of the rods is at 45° with respect to the crossed polarizer and analyzer, one has the best compromise between the induced dipole and the magnitude of its component that is passed by the

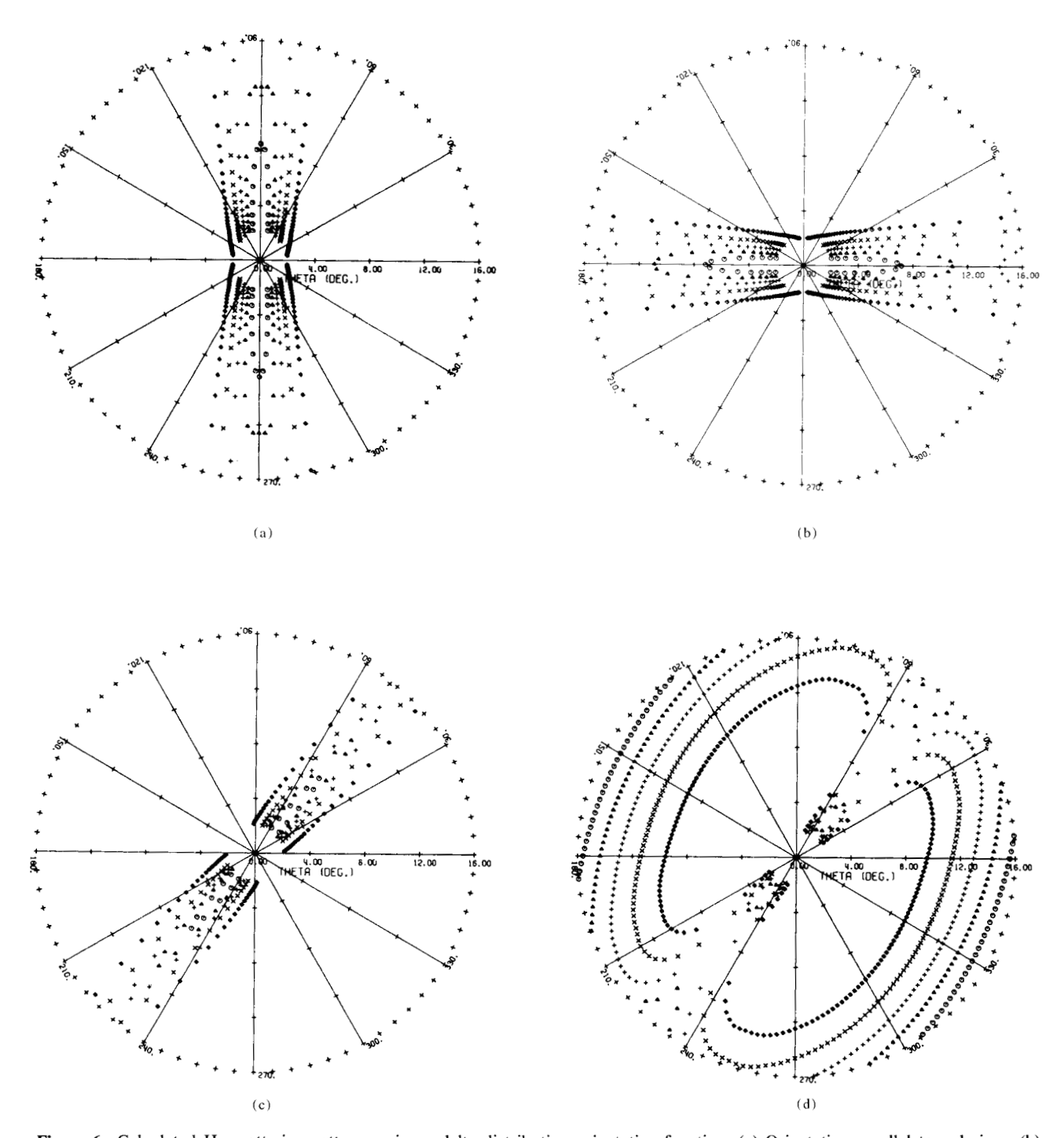


Figure 6 Calculated H_v scattering patterns using a delta distribution orientation function. (a) Orientation parallel to polarizer; (b) orientation perpendicular to polarizer; (c) orientation at 45° to polarizer, retardation = 0.7843; and (d) orientation at 45° to polarizer, retardation = 13.3338.

analyzer. Thus the increased scattering intensity observed in Fig. 5(c) suggests that the optic axis of the rods is oriented either parallel or perpendicular to the long direction of the rods. The slow axis of these rods was determined to be in the long direction. This observation further

suggests that the liquid crystal domain is aligned parallel to the rods. Second, the uniaxial orientation of the rods causes macroscopic polarizability anisotropy. This means that the sample is birefringent. The scattering pattern from such a sample can be significantly altered when the polarization direction of the incident beam does not coincide with the principal optic axes of the birefringent sample [21, 22]. Sample cell C was found to be highly birefringent with a retardation greater than two wavelengths and the slow axis lying along the lapping direction. Thus, the scattering pattern is expected to be altered due to the birefringence effect. Calculated scattering patterns with birefringence effect included [21] are shown in Figs. 6(c) and 6(d). In the calculations, the same rod orientation distribution function was used, and retardation values of 0.7843 and 13.3338 radians were used for Figs. 6(c) and 6(d), respectively. It is noted that for a small value of retardation, the scattering pattern is not much affected but is of a much higher intensity than those calculated for Figs. 6(a) and 6(b). When the retardation is large, the basic long scattering streaks still remain [Fig. 6(d)] and a much diffused scattering pattern is shown at wide angles in, at least, qualitative agreement with the experimental observations described before.

The structures in sample cell C can thus be interpreted as having a uniaxially oriented rod structure in which the liquid crystal is aligned parallel to the long direction of the rod. The unusually long structure must be due to the formation of long microgrooves on the surface, due to lapping, in which the liquid crystals can be aligned. Such highly preferred orientation in one direction also causes the sample to be highly birefringent.

The scattering patterns from sample cell D are shown in Figs. 7(a)-(d). Figures 7(a) and 7(b) are H_v and V_v scattering patterns, respectively, covering scattering angles θ (see Fig. 1), of 25°. Both patterns consist of a low-angle pattern and a wide-angle pattern. The wide-angle patterns are located in between θ s of 15 and 20° while the lowangle patterns cover about 4°. The enlarged low-angle H_v and V, patterns are shown in Figs. 7(c) and 7(d), respectively. The low-angle H_v pattern clearly shows a cloverleaf pattern with an intensity maximum in each lobe along $\mu = 45^{\circ}$, 135°, etc. (see Fig. 1 for definition of μ), suggesting that the scattering is from anisotropic spherulites [16]. The photomicrograph of the sample, shown in Fig. 8, confirms the existence of such a structure. The size of the structure as measured from Fig. 8 is of the order of 30 \approx 40 μ m, which is greater than the thickness of the sample. Thus, the spherulitic structure is two-dimensional. Light scattering theory for two-dimensional spherulites [23] shows that the maximum scattering angle, θ_m , can be related to the average size of the spherulites by the relationship $4\pi (R/\lambda)\sin (\theta_m/2) = 3.9$, where R is the radius of the spherulite and λ is the wavelength of the light within the medium. The θ_m in Figs. 7(a) and 7(c) was measured with a photometric scattering apparatus [24] and found to be at 1.73°. The calculated average spherulite diameter was 35 µm, in agreement with the size observed in the photomicrograph. In addition to the well-defined low-angle

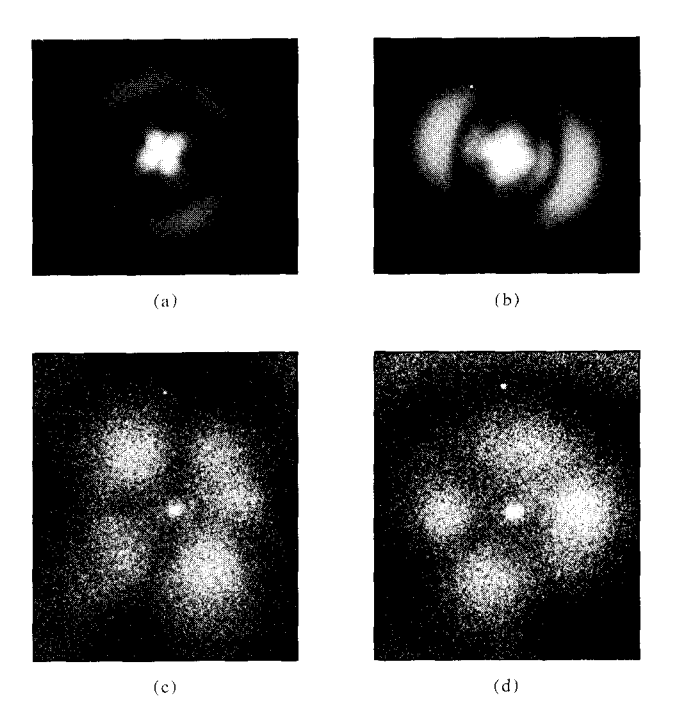
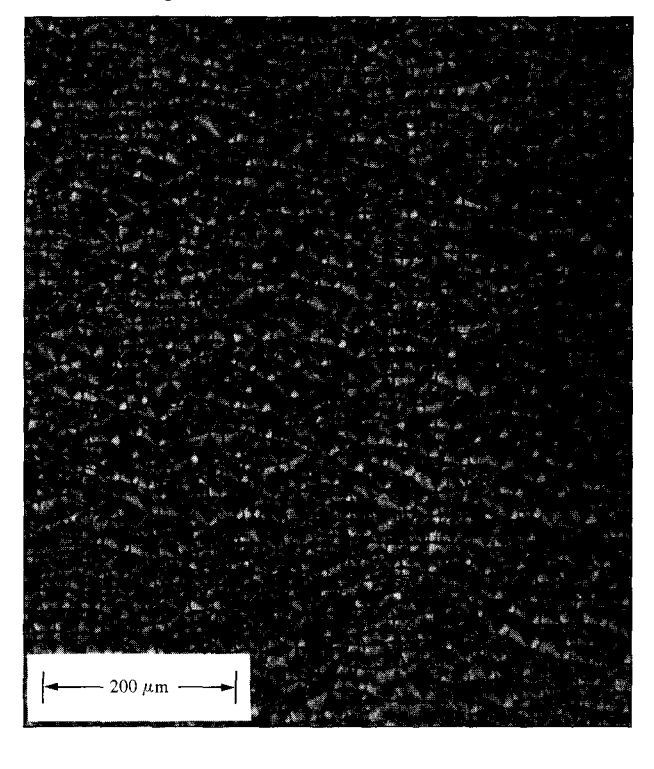
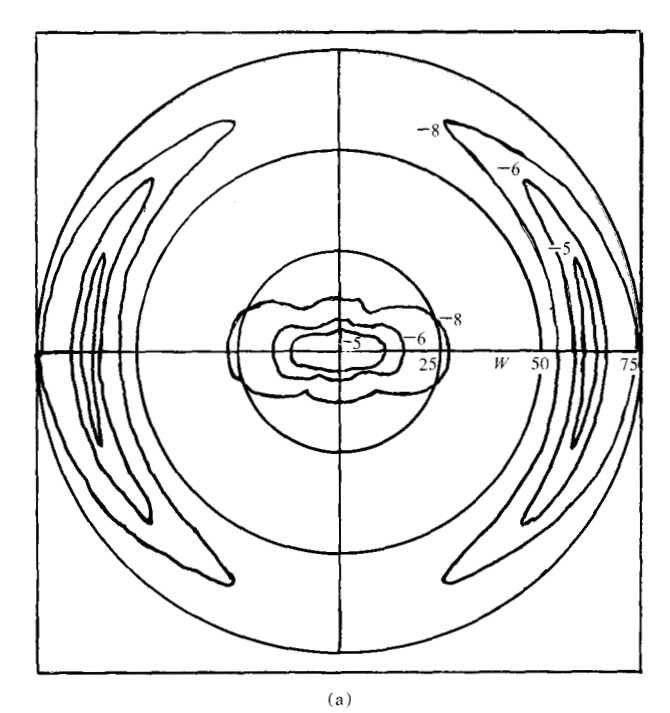


Figure 7 Light scattering patterns from a mixed-alignment sample. (a) Wide-angle H_{ν} ; (b) wide-angle V_{ν} ; (c) low-angle H_{ν} ; and (d) low-angle H_{ν} .

Figure 8 Photomicrograph of mixed-alignment sample in between crossed polaroids.





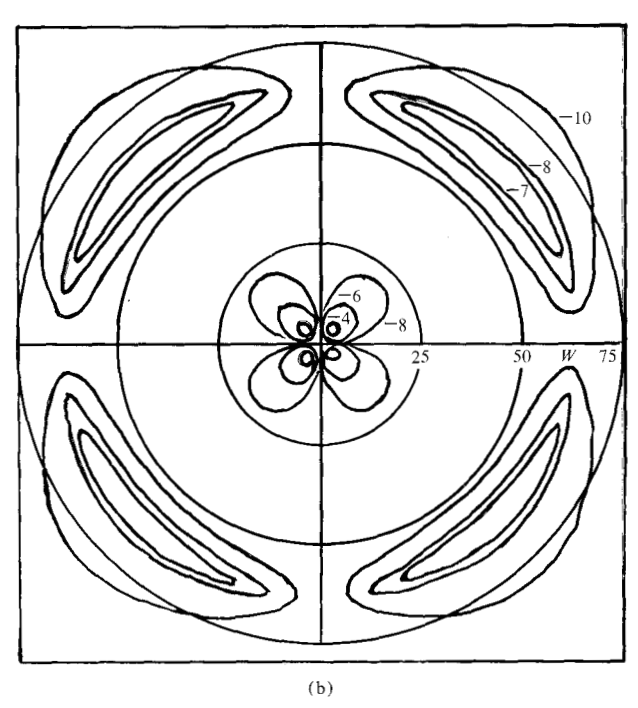


Figure 9 Calculated scattering patterns for two-dimensional banded spherulites (a) V_v and (b) H_v (from [17]).

scattering patterns resulting from spherulites, higher order diffraction peaks can be observed in both H_v and V_v with a much higher intensity associated with the V_v peaks. Such diffraction peaks have also been observed from polyethylene spherulites and are attributed to the periodical twisting of optic axis within the spherulites

[16, 25]. The periodical change in optic axis orientation gives rise to a banded appearance of the spherulites, as shown in Fig. 8. The scattering patterns from such spherulites have been calculated [17] and are shown in Figs. 9(a) and 9(b). For these figures, W is defined as W = $(2\pi R/\lambda)\sin\theta$, a function of the scattering angle θ . The numeral at each contour represents the scattered light intensity in logarithmic scale. The calculation predicts a much stronger scattering intensity associated with the V_y diffraction peak than with the H_u peak. The experimental patterns observed in Figs. 7(a) and 7(b) agree well with the theoretically calculated patterns, indicating that the structure in sample cell D consists of these twisting optic axis spherulites. The explicit description of how the liquid crystal is oriented to give a periodic change in orientation of the optic axis cannot be obtained by the light scattering results. Nevertheless, such a twisted structure can only be observed in the mixed-alignment cell. In the mixedalignment cell, the orientation of the liquid crystal must change from a parallel alignment at one surface to a perpendicular alignment at the other surface. Such a change in orientation must have affected the packing of liquid crystal in such a way as to give a periodic optic axis orientation.

Another observation noted in the mixed-alignment cell is that the size of the superstructure is smaller than that observed in sample cells B and C. This may be attributed to the fact that the change in orientation of liquid crystal from one surface to the other surface in the mixed-alignment cell can cause discontinuities or defects in orientation. Such orientation fluctuations may act as nuclei for crystal growth. The increased number of nuclei results in more crystalline domains but with a smaller size due to the impingement from the growth of neighboring crystal domains. The periodic twisting of crystallites within the spherulites also seems to produce superstructures with more order, as the scattering intensity from the mixedalignment cell was found to be much stronger than that observed from sample cells B and C. A better ordered structure usually results in a more effective polarizability anisotropy, which gives rise to stronger scattering.

• Effect of sample thickness

In the wedge-shaped sample cell, four regions were studied. They are designated E1 through E4 with thicknesses of 1.73, 5.08, 8.64, and 12.70 μ m respectively. The H_v patterns from these four regions are shown in Figs. 10(a)–(d). The exposure time for each pattern was different, with decreasing exposure time for increasing sample thickness in order to show the low angle pattern. Otherwise the patterns in E3 and E4 would be washed out due to overexposure. All these patterns show a low-angle spherulitic scattering pattern and a high order diffraction peak, indicating that they all have the twisted spherulitic

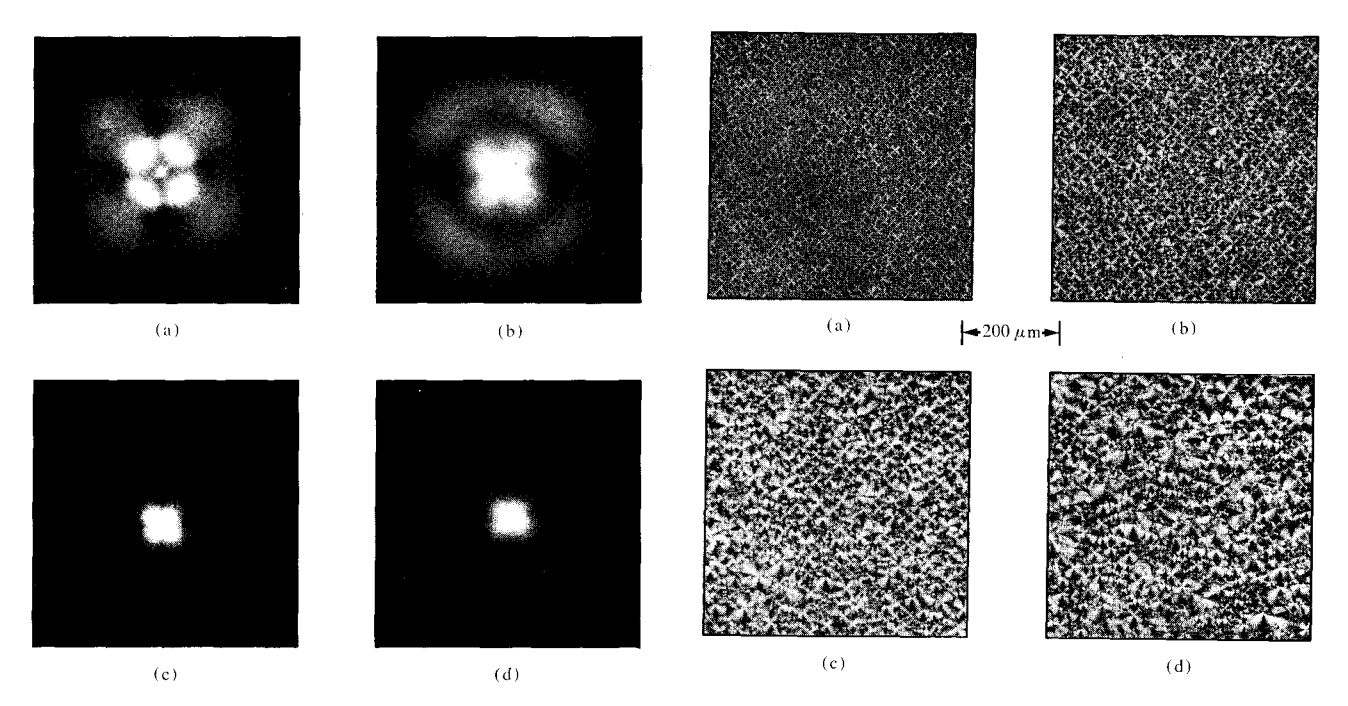


Figure 10 H_v scattering patterns from a wedge-shaped cell. Cell thicknesses are (a) 1.73 μ m, (b) 5.08 μ m, (c) 8.64 μ m, and (d) 12.70 μ m.

Figure 11 Photomicrographs from a wedge-shaped cell. Cell thicknesses are (a) 1.73 μ m, (b) 5.08 μ m, (c) 8.64 μ m, and (d) 12.70 μ m.

structure. The $\theta_{\rm m}$ is different in each pattern and was photometrically measured. The calculated average radius of the spherulites based on different $\theta_{\rm m}$ values is 6.2, 7.0, 10.8, and 13.2 μ m for E1 through E4, respectively. These spherulites of different sizes are also clearly shown in Figs. 11(a)-(d). The increase in spherulite size with increased sample thickness has also been observed by Jabarin and Stein in cholesteryl myristate [6, 7]. They concluded that the nucleation is strongly affected by the surface and the nucleation rate is less for the thicker sample resulting in large structures. In the mixed-alignment cell, when the sample thickness becomes greater and the surface effect becomes less influential, the change in orientation of liquid crystal becomes less drastic and results in fewer nuclei and slower nucleation rate. The overall scattering pattern and the high-order diffraction peak in Figs. 10(a)-(d) become more diffuse with increasing sample thicknesses. The diffuseness can be due to an increase in multiple scattering with increasing sample thickness or due to the existence of disorder within the spherulite as has been observed in polyethylene [26–28]. In a separate experiment, we noted that the scattering pattern from two stacked thin cells was not as diffuse as that from a thick cell of comparable thickness. Therefore, the diffuseness associated with the thick cell was attributed greatly to the presence of disorder. The disorder can result from fluctuations in the optic axis orientation and in the polarizability anisotropy. Since the mixed alignment produces

better ordering within the spherulite due to the surface effect, the thicker samples are less affected by the surface and thus can have more disorder. Also, the thicker samples contain larger structures in which the probability that the optic axis orientation deviates from perfect order certainly becomes greater during the crystallization. Therefore, the effect of thickness on the structure is directly related to the surface effect.

• Effect of thermal history

The effect of superheating on structures was observed by heating a sample to 10, 20, and 30 K above the $T_{\rm NI}$, cooling slowly to the smectic state, and then checking for any structure changes. For all samples, no structural change due to superheating could be observed.

In a cross-linked polyethylene, a spherulitic scattering pattern can be observed even when the polymer is in the melt state. The pattern disappears only when the material is superheated [29]. This indicates that the structural order can persist into the melt and is destroyed when superheated. Such a behavior was not observed from the liquid crystal samples, since no scattering could be observed as soon as the samples were in the melt state. That the same structure was observed after the samples were cooled from the superheated melt indicates that the nucleation must be related to the surface effect.

The structures in these samples are strongly affected by the rate of cooling. In Figs. 12(a)–(d), the H_v scattering



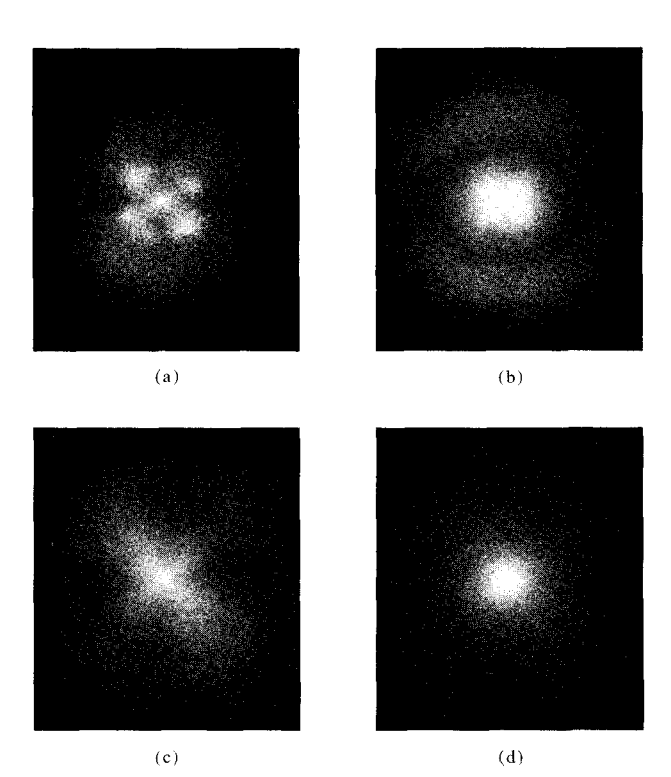


Figure 12 H_v scattering from a quenched wedge-shaped cell. Cell thicknesses are (a) 1.73 μ m, (b) 5.08 μ m, (c) 8.64 μ m, and (d) 12.70 μ m.

patterns from the fast-cooled sample cell E show the change in scattering as compared to those in Figs. 10(a)— (d). In general, the scattering from the fast-cooled sample is much more diffuse. In Figs. 12(a) and 12(b), the scattering from E1 and E2 still shows the clover-leaf spherulitic scattering pattern; however, in Figs. 13(a) and 13(b), the well-defined spherulites can no longer be observed in the photomicrographs. This means that the structure in E1 and E2 still has a spherulitic symmetry but does not have a well-defined shape. The size of these domains remains about the same as in the slow-cooled samples, as judged by the θ_m from these patterns. In these thinner samples, E1 and E2, the surface effect is strong and thus the spherical symmetry in the structure is preserved. However, as the sample was fast cooled from a less ordered state, the nematic phase, some disorder must have been frozen in, forming disordered spherulites which give rise to the diffuse scattering patterns. In Fig. 12(c), the spherulitic pattern is lost and the pattern assumes the characteristics of scattering from rodlike or disklike structures, i.e., a fourfork pattern with scattering intensity decreasing monotonically with increasing scattering angles. In this thicker sample, as the surface effect is less prominent, the frozenin disorder prevents the formation of large spherical symmetrical domains. However, over a smaller distance, the liquid crystals still can align so that their optic axes are

correlated in one direction. It cannot be determined whether the optic axes are parallel (rodlike) or perpendicular (disklike) to the longer direction because the $V_{\rm v}$ scattering pattern is very diffuse. In such a disordered system, the $V_{\rm v}$ pattern consists of a larger contribution from density fluctuation scattering, which is cylindrically symmetrical about the incident beam. Thus, any polarization-dependent scattering from orientation fluctuation is masked.

The H₀ pattern from sample E4 is shown in Fig. 12(d). The pattern has lost its fourfold symmetry and is cylindrically symmetrical about the incident beam. Such a pattern is expected from structures with "random orientation fluctuation" [19] in which the correlated domains are randomly oriented (see Fig. 4). In this thick sample, as the surface effect became even less effective, the amount of frozen-in disorder must have prevented the formation of structures with preferred orientation. Thus, in sample E4, only randomly oriented correlated domains are formed. Judging by the slow decrease in scattered light intensity with increased scattering angle, one can also conclude that the size of these domains is quite small compared with the superstructures observed in the slowcooled samples. The increasing disorder caused by faster cooling rates can also be seen in the photomicrographs of Figs. 13(a)–(d).

As described earlier, sample cell A scattered little light when it was slowly cooled to the smectic state from the nematic state. Thus, the photomicrograph shown in Fig. 14(a) appears dark (sample between crossed polaroids). However, when the sample was rapidly quenched, one can observe small scattering structures formed [Fig. 14(b)]. The H_v scattering pattern (not shown) was similar to that of Fig. 12(d), indicating a "random-orientation-fluctuation"-type structure. Evidently, the fast quenching trapped the disorder during cooling from the nematic state before the surface force could align the liquid crystal to form the homeotropic structure.

The effect of cooling on the structures of liquid crystal is similar to that in crystallization of polymers; i.e., a faster cooling results in smaller and less ordered structures. During polymer crystallization, the packing of molecules depends on thermal fluctuations and the interaction between molecules. In liquid crystals, the packing must be additionally dependent upon the surface effect, which can provide ordering during crystallization. Thus, structures observed in liquid crystals are usually much more regular than those observed in crystalline polymers.

Conclusions

The structures in smectic liquid crystal cells have been characterized by using the light scattering theories developed for crystalline polymers. The surface effect is the predominant force in determining the structures in the

smectic phase. In a polyfluorocarbon-coated cell, the liquid crystals are aligned homeotropically to form a structure with a small cross section. In a SiO₂-coated cell, large fanlike structures are formed in which the liquid crystal tends to align parallel to the radial direction and form smaller fiberlike correlated domains. When the cell surface is lapped, the liquid crystal tends to align parallel to the lapping directions and to form uniaxially oriented rods of a few hundred micrometers in length. The uniaxial orientation of these rods causes the cell to be macroscopically birefringent and thus the light scattering from the cell is strongly dependent upon the polarization direction of the incident light beam. When the cell is coated with polyfluorocarbon on one surface and SiO, on the other surface, two-dimensional spherulites of 30~40 μm in diameter are formed. Because of the different treatments to the surface, the liquid crystal changes its orientation from parallel to the SiO₂-coated surface to perpendicular to the polyfluorocarbon surface. The change in orientation causes a twisting of optic axes within the spherulites and gives the spherulites a banded appearance. These spherulites seem to have better internal order than the other cells, as the scattering from this mixed-alignment cell is stronger than that from the other cells.

The effect of cell thickness on the structure is directly related to the surface effect. When the cell is thin and the surface effect is strong, more ordered structures are formed. The crystallization of liquid crystal is similar to that of polymers; i.e., quenching produces smaller and less ordered structures. However, the structures formed are still highly dependent on the surface effect.

It should be noted that the structure determined by the light scattering methods is of long-range order. The size of the ordered domains is at least comparable to the wavelength of the incident light. The subtle structural difference between a smectic A and smectic B phase, for example in p-aminoazobenzene, thus cannot be differentiated because both phases give the same scattering patterns [8]. However, light scattering provides structural information averaged over the thickness of the sample, which is difficult to obtain from microscopy, especially if the sample is so thick that surface structures dominate the results.

Acknowledgments

The authors acknowledge J. A. Logan for his assistance in photomicroscopy and R. M. Gibson for cell construction. The discussions with E. M. Barrall, II and D. Y. Yoon are much appreciated.

References

- 1. G. W. Gray, Molecular Structure and the Properties of Liquid Crystals, Academic Press, Inc., New York, 1962.
- P. G. de Gennes, The Physics of Liquid Crystals, Clarendon Press, Oxford, England, 1974.

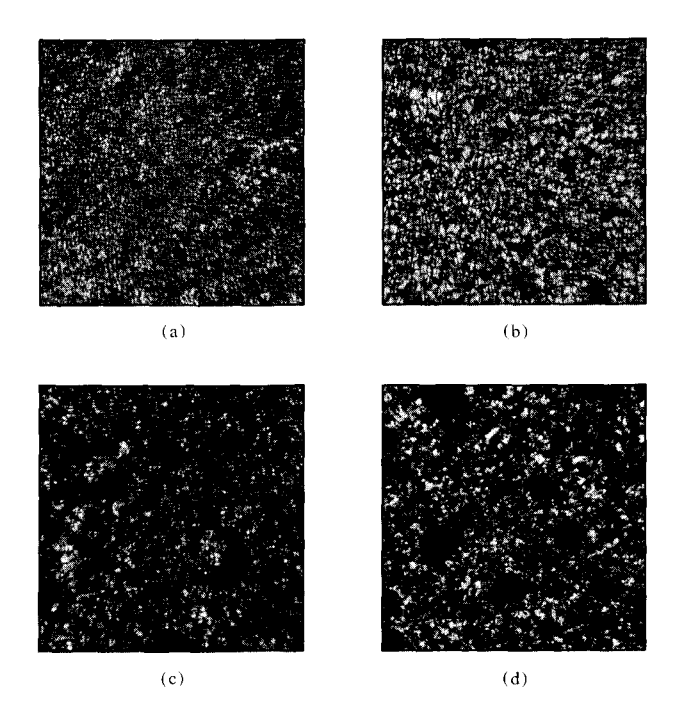


Figure 13 Photomicrographs from a quenched wedge-shaped cell. Cell thicknesses are (a) 1.73 μ m, (b) 5.08 μ m, (c) 8.64 μ m, and (d) 12.70 μ m.

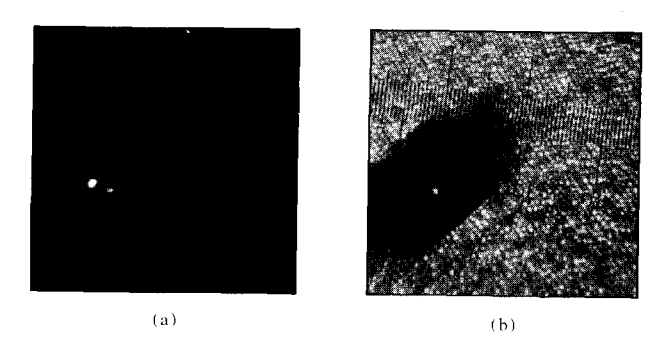


Figure 14 Photomicrographs from a homeotropically aligned cell: (a) slowly cooled; and (b) quenched.

- 3. R. S. Stein, paper presented at the 16th Microsymposium: Advances in Scattering Methods, Prague, Czechoslovakia, July 12–16, 1976.
- R. S. Stein, M. B. Rhodes, and R. S. Porter, J. Colloid Interface Sci. 27, 336 (1968).
- M. B. Rhodes, R. S. Porter, W. H. Chu, and R. S. Stein, Mol. Cryst. Liq. Cryst. 10, 295 (1970).
- 6. S. A. Jabarin and R. S. Stein, J. Phys. Chem. 77, 399 (1973).
- 7. S. A. Jabarin and R. S. Stein, J. Phys. Chem. 77, 409 (1973).
- 8. A. Takase, S. Sakagami, and M. Nakamizo, Mol. Cryst. Liq. Cryst. 22, 67 (1973).
- 9. T. Asada, Kyoto Daigaku Nippon Kagakuseni Kinkyusho Koenshu (Japan) 31, 1 (1974).
- G. J. Sprokel and R. M. Gibson, paper presented at the International Meeting on Liquid Crystals, Kent State University, Ohio, 1976.
- 11. F. J. Kahn, Appl. Phys. Lett. 22, 111 (1973).

- R. S. Stein, Electromagnetic Scattering, M. Kerker, ed., Pergamon Press, Inc., New York, 1963.
- M. B. Rhodes and R. S. Stein, J. Polymer Sci. (Part A-2) 7, 1539 (1969).
- D. Y. Yoon, Ph.D. Thesis, University of Massachusetts, Amherst, Massachusetts, 1973.
- S. Tatematsu, N. Hayashi, S. Nomura, and H. Kawai, *Polymer J.* 3, 488 (1972).
- 16. R. S. Stein and M. B. Rhodes, J. Appl. Phys. 31, 1873 (1960).
- R. S. Stein, P. F. Erhardt, J. J. van Aartsen, S. B. Clough, and M. B. Rhodes, J. Polymer Sci. 18, 1 (1966).
- R. S. Stein, P. F. Erhardt, S. B. Clough, and G. Adams, J. Appl. Phys. 37, 3980 (1966).
- 19. R. S. Stein and P. R. Wilson, J. Appl. Phys. 33, 1914 (1962).
- G. W. Gray, K. J. Harrison, and J. A. Nash, *Pramana Suppl.* 1, 381 (1975).
- W. H. Chu and D. Y. Yoon, Paper presented at the 16th Microsymposium: Advances in Scattering Methods, Prague, Czechoslovakia, July 12-16, 1976.
- 22. M. Hayashi, Y. Murakami, M. Moritani, T. Hashimoto, and H. Kawai, *Polymer J.* 4, 560 (1973).

- S. B. Clough, J. J. van Aartsen, and R. S. Stein, J. Appl. Phys. 36, 3072 (1965).
- W. H. Chu and D. E. Horne, J. Polymer Sci. (Phys. Ed.) 15, 303 (1977).
- 25. S. B. Clough and R. S. Stein, J. Appl. Phys. 38, 4446 (1967).
- R. S. Stein and W. H. Chu, J. Polymer Sci. (Part A-2) 8, 1137 (1970).
- T. Hashimoto and R. S. Stein, J. Polymer Sci. (Part A-2) 9, 1747 (1971).
- D. Y. Yoon and R. S. Stein, J. Polymer Sci. (Phys. Ed.) 12, 763 (1974).
- 29. R. S. Stein, private communication, July 1976.

Received March 23, 1977; revised June 13, 1977

The authors are located at the IBM Research Division laboratory, 5600 Cottle Road, San Jose, California 95193.